

Absence of Long-Range Coherence in the Parametric Emission from Photonic Wires

M. Wouters^{1,2} and I. Carusotto¹

¹*BEC-CNR-INFM and Dipartimento di Fisica, Università di Trento, I-38050 Povo, Italy*

²*TFVS, Universiteit Antwerpen, Universiteitsplein 1, 2610 Antwerpen, Belgium*

We analytically investigate the spatial coherence properties of the signal emission from one-dimensional optical parametric oscillators. Because of the reduced dimensionality, quantum fluctuations are able to destroy the long-range phase coherence even far above threshold. The spatial decay of coherence is exponential and, for realistic parameters of semiconductor photonic wires in the strong exciton-photon coupling regime, it is predicted to occur on an experimentally accessible length scale.

PACS numbers: 42.25.Kb, 42.65.Yj, 71.36.+c, 89.75.Kd

A central concept in the theory of nonlinear dynamical systems is the so-called pattern formation phenomenon, where a spatially ordered structure appears in an otherwise homogeneous system when this is driven far from thermodynamical equilibrium [1]. Very important examples of pattern formation are found in the transverse dynamics of nonlinear optical systems [2, 3], e.g. lasers, bistable devices, as well as planar optical parametric oscillators (OPOs).

In OPOs, the pattern formation phenomenon manifests itself as the appearance of two additional coherent beams, called the signal and the idler, originating from nonlinear conversion of the pump beam when the intensity of this is brought beyond a threshold value [4]. An interesting point of view on OPO operation is provided by the analogy with the Bose-Einstein condensation phenomenon of equilibrium statistical mechanics [5]: as it happens for the matter Bose field in the condensate mode when the temperature is lowered below the condensation temperature, the population of the signal/idler modes becomes macroscopic above the threshold and the field becomes coherent. Although many aspects of the OPO operation are successfully interpreted in terms of concepts of equilibrium statistical mechanics [6, 7], care has to be paid as a non-equilibrium steady state is fundamentally different from a thermodynamical equilibrium state: it is in fact determined by a dynamical equilibrium between external driving and dissipation and does not follow a simple thermal Boltzmann law [8, 9].

At equilibrium, it is well known that long-wavelength fluctuations of both thermal and quantum origin can destroy long-range phase coherence in reduced dimensionality Bose systems, thus replacing true Bose-Einstein condensates with *quasi*-condensates [5, 10, 11]. First studies for the non-equilibrium case have been recently published in an optical context [7, 12, 13] pointing out several analogies with the equilibrium case, but the peculiarities of the non-equilibrium case have not been fully appreciated yet nor experimentally investigated. The aim of the present Letter is to contribute to fill this gap: although the theory we develop for reduced-dimensionality effects in non-equilibrium systems is fully general, we focus our

discussion on a specific system in which the effects we predict are experimentally accessible.

We consider planar semiconductor microcavities in the strong-coupling regime [14, 15], in which OPO operation has been recently observed [16, 17]. The extremely large value of the excitonic nonlinearity is responsible for the ultra-low OPO threshold of these systems, which suggests an enhanced role of quantum fluctuations. By nanostructuring planar cavities, reduced dimensionality *photonic wires* can be obtained, without spoiling the strong-coupling condition, nor the possibility of OPO operation [18]. All these facts make these systems an ideal candidate for the study of quantum effects on pattern formation in non-equilibrium systems, in particular low-dimensional ones.

The photonic states in photonic wires (Fig.1a) are quantized in both the growth z and the transverse y directions, leading to many subbands. The dispersion of the j th subband as a function of the longitudinal wavevector k along the x direction is approximately given by $\omega_{Cj}(k) = \omega_C^0 \sqrt{1 + (k^2 + k_{y,j}^2)/k_z^2}$, where $k_{y,j}$ and k_z are the quantized photon wavevectors in respectively the y and z directions. The strong dipole coupling between cavity photons and the quantum well exciton (almost dispersionless at ω_X^0) results in a Rabi frequency Ω_R larger than the damping rates so that the eigenmodes of the system at linear regime are polaritons, i.e. coherent superpositions of cavity-photonic and excitonic modes. Among the polaritonic subbands, we only keep the three lowest ones denoted by $j = s, p, i$, whose dispersion $\varepsilon_j(k)$ is plotted for an example of realistic experimental parameters in Fig.1b. As experimentally shown in [18], the photonic wire geometry introduces a TE/TM splitting of the different polarization states of each subband, large enough for the OPO process to take place on a single polarization state only, while almost no emission takes place in the other one. As its effect on the dynamics is small, it will be safely neglected in the following of this Letter. For simplicity, we shall also neglect the weak k -dependence of both the Hopfield coefficients $U_{X,C}^j$ quantifying the excitonic and cavity-photonic weights of each

polariton subband $j = s, p, i$ as well as of the corresponding transverse photonic wave functions $\phi_{\perp}^j(y)$.

As discussed in detail in [7], a simple, yet quantitative description of the dynamics of the polariton quantum field in a microcavity is based on a Wigner representation of the quantum fields in terms of classical, yet *stochastic* \mathbf{C} -number polariton fields $\phi_{j=s,p,i}(x)$. In the Wigner framework, the time-evolution of the polariton field is described in terms of stochastic differential equations, which in Fourier space read:

$$i d\phi_j(k) = \left\{ [\varepsilon_j(k) - \frac{i}{2}\gamma_j(k)]\phi_j(k) + 2\pi U_C^p \delta_{jp} \delta(k) F_L e^{-i\omega_L t} \right. \\ \left. + \sum_{j'} \int \frac{dk'}{2\pi} \mathcal{E}_{jj'}(k, k') \phi_{j'}(k') \right\} dt + \sqrt{\frac{\gamma_j(k)}{4}} dW_j(k, t), \quad (1)$$

The damping rate $\gamma_j(k)$ accounts for radiative and non-radiative losses of both the excitonic and photonic components of the polaritons. In the region of interest, it has a weak dependence on k [24]. As usual [19], damping is intimately connected to the presence of quantum fluctuations. These show up in the Wigner formalism as Gaussian, complex-valued, white noise terms $dW_j(k, t)$ satisfying

$$\overline{dW_j(k, t) dW_{j'}(k', t)} = 0 \quad (2)$$

$$\overline{dW_j(k, t) dW_{j'}^*(k', t)} = 4\pi dt \delta(k - k') \delta_{jj'}. \quad (3)$$

Expectation values of observables will be obtained as averages over the noise $dW_j(x, t)$. Exciton-exciton collisional interaction are modeled by a repulsive contact potential with strength g . The mean field energy can then be simply written as

$$\mathcal{E}_{jj'}(k, k') = \sum_{r,s} \int \frac{dp}{2\pi} g_{1D}^{jrj's} \phi_r^*(p - k) \phi_s(p - k') \quad (4)$$

in terms of the overlap integrals of the excitonic component of the transverse wave functions $\phi_{X\perp}^j(y) = U_X^j \phi_{\perp}^j(y)$ of the different subbands:

$$g_{1D}^{jrj's} = g \int dy \phi_{X\perp}^{j*}(y) \phi_{X\perp}^{r*}(y) \phi_{X\perp}^{j'}(y) \phi_{X\perp}^s(y). \quad (5)$$

To inject polaritons, a coherent and monochromatic pump laser of frequency ω_L and amplitude F_L is shone onto the cavity. In the x direction the pump beam is taken as homogeneous with a constant phase, while its profile along y is chosen in a way to have a negligible overlap with all subbands but for the p one. This results in a coherent injection of $k = 0$ polaritons into the p subband only.

Because of nonlinear interactions, two *pump* polaritons in the central p subband can then be converted into one *signal* polariton in the s subband and one *idler* polariton

in the i subband. The *mean-field* solution neglecting the noise terms in (1) has the simple plane wave structure:

$$\phi_j^o(x) = \sqrt{\rho_j^o} e^{i(k_j x - \omega_j t + \theta_j)}. \quad (6)$$

At low pump intensities, a stable solution with a finite density in the pump mode only (i.e. $\rho_s^o = \rho_i^o = 0$) exists. The wavevector $k_p = 0$, as well as the frequency $\omega_p = \omega_L$ are fixed by the external laser; in particular, we have chosen ω_L to be just below the bottom of the p subband so as to avoid complicated pump bistability effects [20, 21]. For increasing pump powers, this solution eventually becomes dynamically unstable above some threshold, and is replaced by a new solution with finite signal and idler intensities $\rho_{s,i}^o$. The pump frequency and wavevector remain the same $\omega_p = \omega_L$ and $k_p = 0$, while many values are possible for the signal/idler frequencies $\omega_{s,i}$ and wavevectors $k_{s,i}$, with the only constraint that $\omega_i = 2\omega_L - \omega_s$ and $k_i = -k_s$ and that the solution is dynamically stable. This latter condition defines a band [1] of stable k_s values and for each of them, the densities $\rho_{s,p,i}^o$ and the frequencies $\omega_{s,i}$ can be simply obtained by substituting the ansatz (6) into the deterministic part of the motion equation (1). The results are plotted in Fig.1c as a function of the pump laser intensity $I_L = |F_L|^2$ for the specific case of a signal wavevector $k_s = 0$, which is the first to become unstable for the chosen parameters. The results would however be qualitatively similar if a finite $k_s \neq 0$ was taken. The signal/idler densities $\rho_{s,i}^o$ continuously grow from zero starting from the lower threshold, get to their maximum value, and then go back to zero at the upper threshold, where we are back to a pump-only mean-field solution $\rho_s^o = \rho_i^o = 0$ [21].

The simplest way to include the effect of noise terms is to linearize the Wigner equation (1) around the mean-field solution (6) and treat the noise as a perturbation. This is best done using the same ansatz:

$$\phi_j(x, t) = \sqrt{\rho_j^o + \delta\rho_j(x, t)} e^{i(k_j x - \omega_j t + \theta_j + \delta\theta_j(x, t))}. \quad (7)$$

as in the generalized density-phase Bogoliubov theory developed for the study of quasi-condensates at equilibrium [10, 11]. This approach does not require the existence of long-distance coherence, but only that density fluctuations are small $|\delta\rho_j| \ll \rho_j^o$, and the signal and idler phases are well defined and locally locked by the parametric process $|2\delta\theta_p - \delta\theta_s - \delta\theta_i| \ll 1$.

Simple Ito manipulations of (1), lead to the linearized motion equation for the fluctuations in frequency space:

$$\omega \mathcal{U}(k, \omega) = \mathcal{L}(k) \mathcal{U}(k, \omega) + \sqrt{\Gamma(k)/4} \mathcal{W}(k, \omega). \quad (8)$$

The fluctuation 6-vector is defined as $\mathcal{U}(k, \omega) = [\mathbf{u}^{(+)}(k, \omega), \mathbf{u}^{(-)}(k, \omega)]^T$, where the 3-vector:

$$\mathbf{u}_m^{(\pm)}(k, \omega) = \frac{\delta\rho_m(k, \omega)}{2\sqrt{\rho_m^o}} \pm i\sqrt{\rho_m^o} \delta\theta_m(k, \omega), \quad (9)$$

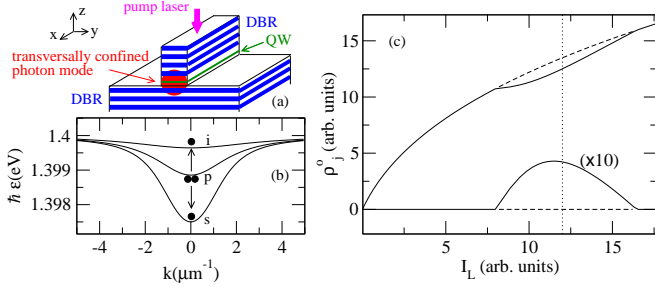


FIG. 1: (a) Sketch of a semiconductor photonic wire with an embedded quantum well (QW). Confinement in the z, y directions is provided by respectively a pair of Distributed Bragg Reflectors (DBR) and a lateral etching of the cavity. (b) Linear regime dispersions of signal, pump and idler subbands and sketch of the parametric process under examination. (c) Exciton density in the pump and signal modes as a function of the pump laser intensity for a given $\hbar\omega_p = 1.398725$ eV. Full (dashed) lines represent linearly stable (unstable) solutions. Cavity parameters inspired by Ref.[18]: $\hbar\omega_C^o = \hbar\omega_X^o = 1.4$ eV, $k_z = 20\mu\text{m}^{-1}$, $\hbar\Omega_R = 2.5$ meV, $L_y = 4\mu\text{m}$, $\hbar g = 5 \times 10^{-6}$ eV μm^2 and $\hbar\gamma_{s,p,i} = 0.15$ meV.

The index m takes here the values 1, 2, 3 corresponding respectively to the subbands s, p, i . The complex-valued noise 6-vector is analogously defined as $\mathcal{W}(k, \omega) = [\mathbf{w}(k, \omega), -\mathbf{w}^*(-k, -\omega)]^T$, and is such that $\langle \mathbf{w}_m^*(k, \omega) \mathbf{w}_n(k', \omega') \rangle = 8\pi^2 \delta_{mn} \delta(k - k') \delta(\omega - \omega')$ and $\langle \mathbf{w}_m(k, \omega) \mathbf{w}_n(k', \omega') \rangle = 0$. The diagonal 6x6 damping matrix $\Gamma(k)$ has $\Gamma_{ll}(k) = \gamma_l(k_l + k)$ for $1 \leq l \leq 3$ and $\Gamma_{ll}(k) = \gamma_{l-3}(k_{l-3} - k)$ for $4 \leq l \leq 6$, while all other elements vanish. The 6x6 matrix $\mathcal{L}(k)$ has the typical Bogoliubov structure

$$\mathcal{L}(k) = \begin{pmatrix} M(k) & Q \\ -Q^* & -M^*(-k) \end{pmatrix}, \quad (10)$$

in terms of the 3x3 matrices $M(k)$ and Q whose elements (for $1 \leq m, n \leq 3$) are given by

$$M_{mn}(k) = [\varepsilon_m(k_m + k) - \omega_m - i\gamma_m(k_m + k)/2] \delta_{m,n} + 2 \sum_{rt} g_{1D}^{mnr} \delta_{m,n+r-t} e^{i(\theta_r - \theta_t - \theta_m + \theta_n)} \sqrt{\rho_r^o \rho_t^o} \\ Q_{mn} = \sum_{rt} g_{1D}^{mnr} \delta_{m+n,r+t} e^{i(\theta_r + \theta_t - \theta_m - \theta_n)} \sqrt{\rho_r^o \rho_t^o}.$$

The eigenvalues of the $\mathcal{L}(k)$ matrix give the excitation spectrum $\lambda_\nu(k)$ of our system around the mean-field steady-state solution. An example of such a spectrum is plotted in Fig.2. Dynamical stability of the mean-field solution requires that for all branches $\text{Im}[\lambda_\nu(k)] < 0$ for all values of k . As the mean-field solution (6) spontaneously breaks the $U(1)$ signal/idler phase symmetry $\theta_{s,i} \rightarrow \theta_{s,i} \pm \Delta\theta$ of the motion equation (1), a Goldstone branch is necessarily present. For clarity, it will be denoted in the following by the index $\nu = G$. Its

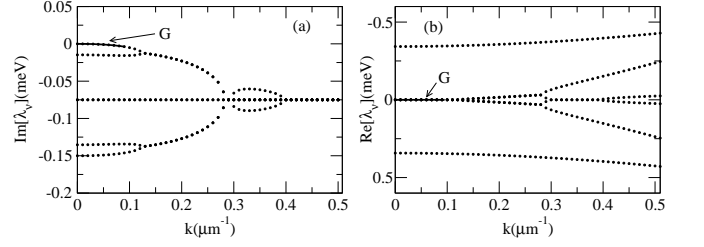


FIG. 2: Imaginary (a) and real (b) parts of the Bogoliubov excitation spectrum around the mean field steady-state. Solid line indicates the Goldstone branch. Pump-intensity as at the dotted line in Fig.1b. Same cavity parameters as in Fig.1.

main property is that its dispersion $\lambda_G(k)$ at $k = 0$ is exactly $\lambda_G(k = 0) = 0$ [1]. The behavior of this eigenvalue $\lambda_G(k)$ in the neighborhood of $k = 0$ is crucial for the long-distance properties of our system. Dynamical stability and analyticity [1, 22] arguments guarantee that for $k \rightarrow 0$ one can expand

$$\text{Im}[\lambda_G(k)] \simeq -k^2/2a, \quad (11)$$

with a strictly positive coefficient $a > 0$: differently from zero-sound in equilibrium Bose gases, the Goldstone mode is here a diffusive, non-propagating mode.

The first-order spatial coherence of the parametric emission is determined by the spatial coherence of the in-cavity polaritons. In the Wigner representation, this can be written for $x_1 \neq x_2$ as:

$$g_s^{(1)}(x_1 - x_2) = \langle \phi_s^*(x_1, t) \phi_s(x_2, t) \rangle_W. \quad (12)$$

Neglecting in (7) the density fluctuations $\delta\rho_j$ which do not contribute to long-distance properties, and expanding higher order correlations by means of the Wick theorem for Gaussian stochastic variables [19], one obtains:

$$g_s^{(1)}(x_1 - x_2) = \rho_s^o e^{ik_s(x_2 - x_1)} e^{-\chi_s(x_1 - x_2)}. \quad (13)$$

where the phase-phase correlation function is defined as:

$$\chi_s(x_1 - x_2) = \frac{1}{2} \langle [\delta\theta_s(x_1, t) - \delta\theta_s(x_2, t)]^2 \rangle_W. \quad (14)$$

This can be evaluated using (8) and (9):

$$\chi_s(x) = \frac{1}{32\pi^2 \rho_s^o} \sum_{\nu\mu} \int d\omega dk \frac{(1 - e^{ikx}) \bar{\Gamma}_{\nu\mu}(k)}{[\omega - \lambda_\nu^*(k)][\omega - \lambda_\mu(k)]}, \quad (15)$$

in terms of the matrix elements

$$\bar{\Gamma}_{\nu\mu}(k) = P^\dagger B_\mu(k) \Gamma(k) B_\nu^\dagger(k) P. \quad (16)$$

The vector $P = (1, 0, 0, -1, 0, 0)^T$ and the matrices $B_\nu(k)$ are projectors on the eigenspace corresponding to the

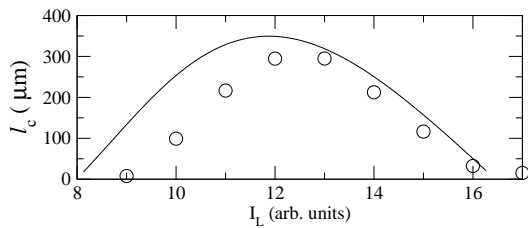


FIG. 3: Analytical prediction (18) (solid) and QMC data (circles) for the coherence length as a function of the pump power. Same cavity parameters as in Fig.1.

eigenvalue $\lambda_\nu(k)$. The frequency integral in (15) can then be performed closing the integration contour in the complex plane:

$$\chi_s(x) = \frac{i}{16\pi\rho_S^0} \sum_{\nu\mu} \int dk (1 - e^{ikx}) \frac{\bar{\Gamma}_{\nu\mu}(k)}{\lambda_\nu^*(k) - \lambda_\mu(k)}. \quad (17)$$

As usual, the large distance properties are determined by the $k \approx 0$ region, and the dominant contribution comes from the Goldstone mode, that is for $\nu = \mu = G$. A simple analytical expression, can be obtained by keeping only this mode, then approximating the smooth function $\bar{\Gamma}_{GG}(k)$ with its $k = 0$ value $\bar{\Gamma}_{GG}^o$ (of the order of the γ 's), and finally extending the integral to infinity. This results in an asymptotic exponential decrease $g_s^{(1)}(x) \propto \exp(-|x|/\ell_c)$, with a coherence length ℓ_c equal to

$$\ell_c = \frac{16\rho_s^o}{a\bar{\Gamma}_{GG}^o}. \quad (18)$$

In Fig.3, ℓ_c is plotted as a function of the pump power. Its behaviour closely follows the one of the signal density ρ_s^o so that ℓ_c goes to 0 at the edges of the OPO region, and has its maximum in the middle. This prediction can be compared to the numerical results of a full Monte Carlo simulation of the Wigner equation as reported in [7]. The agreement is good and the small quantitative discrepancy is mostly due to the three-mode expansion performed here, which does not take into account the upper polariton.

It is instructive to compare the non-equilibrium formula (18) with the equilibrium one $\ell_c^{eq} = 2n\hbar^2/k_B T m$ for a degenerate 1D Bose gas of density n at temperature T . The dependence on the density is the same in the two cases, while the role of the temperature T is played in the non-equilibrium case by the noise associated to damping. Another, more striking, difference concerns the free boson mass m , which is replaced in the non-equilibrium case by the parameter a defined in (11), i.e. the inverse of the second derivative of the *imaginary* part of the Goldstone mode dispersion.

For a given value of the interaction energy $g\rho_j$ and all detuning and cavity parameters kept fixed, the co-

herence length has the remarkable scaling $\ell_c \propto 1/g$. The extremely high value of the excitonic nonlinearity as compared to OPOs based on conventional nonlinear optical media [6, 12, 23] implies that the effect of quantum fluctuations is strongly enhanced. In particular, one can observe in Fig.3 that the predicted coherence length is of the order of hundred microns for realistic experimental parameters, which means that it should be within experimental reach for current semiconductor technology. In addition to their interest for the fundamental physics of pattern formation and non-equilibrium phase transitions, the conclusions of the present Letter may also have significant consequences for device applications of OPOs, as quantum fluctuations provide an intrinsic limitation to the long distance phase coherence, even in the absence of other decoherence and disorder effects.

Continuous stimulating discussions with C. Ciuti, J. Tignon, C. Diederichs, and A. Rosso are warmly acknowledged. This research has been supported financially by the FWO-V projects Nos. G.0435.03, G.0115.06, and the Special Research Fund of the University of Antwerp, BOF NOI UA 2004. M.W. acknowledges financial support from the FWO-Vlaanderen in the form of a “mandaat Postdoctoraal Onderzoeker”.

-
- [1] M. C. Cross and P. C. Hohenberg, *Rev. Mod. Phys.* **65**, 851 (1993).
 - [2] L.A. Lugiato, M. Brambilla and A. Gatti, *Adv. At. Mol. Opt. Phys.* **40**, 229 (1998).
 - [3] K. Staliunas, *Transverse Patterns in Nonlinear Optical Resonators* (Springer, 2003).
 - [4] D. F. Walls and G. J. Milburn, *Quantum Optics* (Springer, 1994).
 - [5] L.P. Pitaevskii and S. Stringari, *Bose-Einstein Condensation*, Clarendon Press Oxford (2003).
 - [6] A. Gatti, L. Lugiato, *Phys. Rev. A* **52**, 1675 (1995).
 - [7] I. Carusotto and C. Ciuti, *Phys. Rev. B* **72**, 125335 (2005).
 - [8] for an introduction, see L. E. Reichel, *A Modern Course in Statistical Physics*, University of Texas Press (1980).
 - [9] *Phase transitions and critical phenomena*, vol.17 (Statistical mechanics of driven diffusive systems), eds. C. Domb and J.L. Lebowitz, Academic, Neq York (1989).
 - [10] V.N. Popov, *Functional Integrals in Quantum Field Theory and Statistical Physics*, Reidel Dordrecht (1983).
 - [11] Y. Castin, *J. Phys. IV France*, **116**, 89 (2004) and references therein.
 - [12] R. Zambrini *et al.*, *Phys. Rev. A* **62**, 063801 (2000).
 - [13] K. Staliunas, *cond-mat/0001436*; K. Staliunas, *Phys. Rev. E* **64**, 066129 (2001).
 - [14] J. Baumberg and L. Via (Eds.) Special issue on Microcavities, [*Semicond. Sci. Technol.* **18**, S279 (2003)].
 - [15] B. Deveaud (Ed.), Special issue on the “Physics of semiconductors microcavities”, *Phys. Stat. Sol. B* **242**, 2145-2356 (2005) and references therein.
 - [16] R. M. Stevenson *et al.*, *Phys. Rev. Lett* **85**, 3680 (2000).
 - [17] R. Houdré *et al.*, *Phys. Rev. Lett.* **85**, 2793 (2000).

- [18] G. Dasbach *et al.*, Phys. Rev. B **71**, 161308(R) (2005).
- [19] C.W. Gardiner and P. Zoller, *Quantum Noise* (Springer, 2004).
- [20] I. Carusotto and C. Ciuti, Phys. Rev. Lett. **93**, 166401 (2004).
- [21] D.M. Whittaker, Phys. Rev. B **71**, 115301 (2005).
- [22] T. Kato, *Perturbation theory for linear operators* (Springer-Verlag, 1984).
- [23] R.L. Sutherland, *Handbook of nonlinear optics* (Marcel Dekker, 2003).
- [24] The k -dependence of the final density of states and of the tunneling matrix element through the DBR cavity mirrors can be safely neglected as long as the characteristic wavevectors $k_{y,j}$ and $1/\ell_c$ of the in-cavity polaritons are well inside the DBR reflection window.